Surface of Sputtered and Annealed Polar $SrTiO_3(111)$: TiO_x-Rich ($n \times n$) Reconstructions

Bruce C. Russell and Martin R. Castell*

Department of Materials, University of Oxford, Parks Road, Oxford OX1 3PH, United Kingdom

Received: November 27, 2007; In Final Form: January 15, 2008

$SrTiO_3(111)$ samples, doped with Nb, are Ar^+ ion sputtered and annealed in ultrahigh vacuum (UHV) and in varying pressures of oxygen and investigated using scanning tunneling microscopy (STM) and Auger electron spectroscopy (AES). STM images show that a number of reconstructions constituting a family of ($n \times n$) surfaces are able to form on the surface by varying the sputtering conditions and O_2 annealing pressures. The family of ($n \times n$) reconstructions is due to variations in the oxygen stoichiometry, with (3×3) the most oxygen-rich, followed by (4×4), (6×6), and finally (5×5). Annealing in atmospheric pressure of air causes a ($9/5 \times 9/5$) reconstruction to form. Highly reducing the surface, through extended UHV annealing, produces a TiO (111)-(2×2) nanophase. Step heights are always found to be equivalent to integer multiples of the distance between two similar (111) planes (the d_{111} lattice parameter). AES analysis indicates no detectable impurities and shows all the surfaces to be Ti-enriched and either stoichiometric or deficient with respect to Sr. The concentration of Ti at the surface increases as the surface becomes more reduced.

1. Introduction

Perovskite titanates show a variety of surface reconstructions due to their ability to accommodate a large range of stoichiometries in the surface region. Strontium titanate is the model system displaying this behavior. $SrTiO_3$ crystallizes, above 105 K, into a cubic structure with a 0.3905 nm lattice parameter and formal ionic charges of Sr^{2+}, Ti^{4+}, and O^{2-}. Ti ions sit at the corners of the cubic unit cell, with O ions positioned halfway along each vertex. A Sr ion is centered in the middle of the unit cell. The $SrTiO_3(111)$ termination is of particular interest because it is a polar surface. Polar surfaces are those where the bulk termination possesses a dipole perpendicular to it. When viewed in the $\langle 111 \rangle$ direction, $SrTiO_3$ is composed of alternating Ti^{4+} and SrO_3^{4-} planes. These alternating positive and negative planes create a macroscopic dipole perpendicular to the surface. The distance between two nearest similar planes (i.e., two Ti planes or two SrO_3 planes) is the d_{111} lattice spacing (0.225 nm). The presence of a perpendicular dipole causes the surface energy of the termination to be infinite.[1] It was originally thought that this dipole would prevent terminations along particular Miller index planes from forming. However, it has now been found that this dipole can be removed via four mechanisms:[2] changing the surface stoichiometry; redistribution of electrons in the surface region; adsorption of atoms or molecules; and faceting (although this, by definition, locally changes the Miller index). These mechanisms generally allow a large number of reconstructions to be formed, with variable compositions and surface chemistry.

In this paper we will build upon previous results which showed that the $SrTiO_3(111)$ surface can be stabilized.[3] When polished and unsputtered $SrTiO_3(111)$ samples are annealed in ultrahigh vacuum (UHV) at 850 °C for 30 min, a surface with coexisting domains of ($\sqrt{7} \times \sqrt{7}$)R19.1° and ($\sqrt{13} \times \sqrt{13}$)-R13.9° reconstructions is formed. None of the reconstructions observed in this paper were found to form on unsputtered surfaces. Step heights between terraces were found to be 0.21 ± 0.02 nm, which corresponds to the d_{111} lattice spacing. This surface was significantly Ti-enriched with respect to stoichiometry, with some additional Sr enrichment. It was proposed that the polarity was removed by the change in stoichiometry at the surface. There are, however, numerous ways of processing the (111) surface, which in turn produce different reconstructions, with different mechanisms for stabilizing the polarity. We will deal with those in this paper.

Few other $SrTiO_3(111)$ reconstructions have been reported. A Ti^{4+}-rich, (4×4) reconstruction was produced by Haruyama et al.[4] by annealing in UHV at 1200 °C for 5 min and studied by low-energy electron diffraction (LEED). Annealing in different gases changes the surface composition. Samples annealed for 10 h at 1000 °C in 1 atm Ar produced a surface with large flat triangular terraces, whereas those annealed for 10 h at 1000 °C in 1 atm O_2 had a trench structure.[5,6] The O_2-annealed surface was more Ti-enriched than the Ar-annealed sample.

Ti enrichment is a common mechanism for stabilizing the $SrTiO_3(111)$ surface. Sputtering the surface at room temperature in UHV and then annealing at 600 °C has been shown to cause an increase in the Ti concentration at the surface.[7] Room-temperature Ar sputtering followed by annealing also causes the $SrTiO_3(100)$ surface to become Ti-enriched, with TiO_x-rich nanostructures,[8−10] a TiO_x-rich $c(4 \times 2)$ reconstruction,[11,12] and anatase[13] all being reported on the surface.

In this paper we present several ($n \times n$) reconstructions, which are formed by Ar^+ ion sputtering the surface prior to annealing. The resultant reconstructions are analyzed using both scanning tunneling microscopy (STM) and Auger electron spectroscopy (AES).

2. Experimental Methods

$SrTiO_3$ single crystals doped with Nb at 0.5% by weight with epi-polished (111) surfaces were supplied by PI-KEM, U.K. $SrTiO_3$ is an insulator with a band gap of 3.2 eV at 25 °C.[14] The addition of Nb dopes $SrTiO_3$ n-type, giving rise to sufficient

* To whom correspondence should be addressed. E-mail: martin.castell@materials.ox.ac.uk.

10.1021/jp711239t CCC: $40.75
Published on Web 04/01/2008

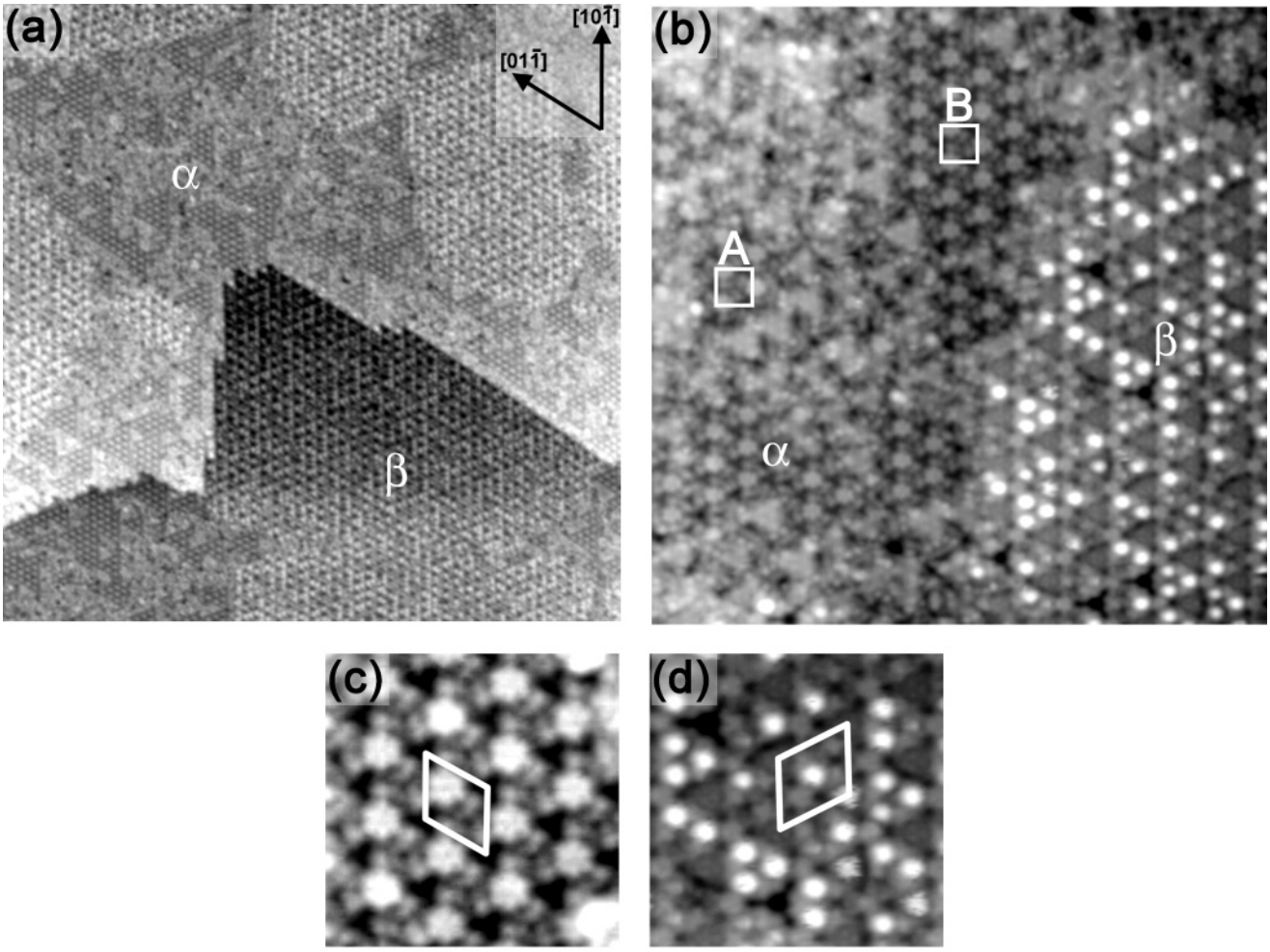

Figure 1. (a) Large-scale STM image showing two terraces separated by a step edge. Both terraces are made up of large domains of the (6 × 6) reconstruction (indicated by β) and regions with smaller domains of (4 × 4) surface (indicated by α) (image size 160 × 160 nm^2, sample bias 2.22 V, tunneling current 0.12 nA). (b) More detailed image showing both the (4 × 4) (α) and (6 × 6) (β) reconstructions. The (4 × 4) surface contains two domains which have similar but different features. These features are indicated by A and B. They are non-superimposable mirror images, and thus, two chiral domains are present (image size 38 × 38 nm^2, sample bias 2.0 V, tunneling current 0.15 nA). (c) Detailed image of the (4 × 4) reconstruction with the chiral unit cell shown in white (image size 9 × 9 nm^2, sample bias 2.0 V, tunneling current 0.5 nA). (d) High-resolution image of the (6 × 6) reconstruction with the unit cell indicated by a white rhombus (image size 13 × 13 nm^2, sample bias 1.86 V, tunneling current 0.17 nA).

electrical conductivity at room temperature for STM experiments to be performed. The crystals were introduced without pretreatment into the UHV chambers of two instruments. These were a JEOL JSTM4500xt which includes STM and LEED analysis facilities and a JEOL JSTM4500s comprising STM, LEED, and a UHV scanning electron microscope (SEM) with a SPECS PHOIBOS 100 electron energy analyzer. The UHV SEM and electron energy analyzer were used in combination to provide Auger electron spectroscopy (AES) at high spatial resolution. Ion sputtering facilities were also present on both instruments. The STM scanner was calibrated using a Si(111) (7 × 7) reconstructed sample. The vacuum on each instrument was regularly observed to be of the order of 10^{-8} Pa. It was possible to leak O_2 into both chambers to allow annealing in different environments. Sample preparation was also carried out at atmospheric pressure by placing the samples into sealed mullite furnace tubes and heating using a tube furnace. Gases at atmospheric pressure were vented through the tube during annealing. Constant current STM images were produced at room temperature using etched Tungsten tips. The samples were annealed in UHV by resistively passing a direct current through the sample, and the temperatures were measured through a viewport with an optical pyrometer.

3. Results

3.1. (6 × 6) and (4 × 4) Reconstructions. Ar ion sputtering a $SrTiO_3$(111) surface at 500 eV for 10 min and subsequently annealing for 30 min at 950 °C in UHV produces the surface shown in Figure 1a. The image consists of two terraces with step edges that predominantly follow the crystallographic ⟨110⟩ directions. After analysis of a number of images, the step heights are found to be 0.217 ± 0.016 nm, which correspond to the d_{111} lattice parameter (0.225 nm). Each terrace is made up of two differently ordered regions which are labeled α and β. The β regions are larger and continuous over a greater area, whereas the α regions are made up of a number of smaller ordered domains with disorder between them.

Figure 1b shows an image with both α and β domains at greater magnification. The periodicity of the α domain is 2.29 ± 0.08 nm, which is approximately four times the underlying unreconstructed periodicity (0.55 nm). Likewise that of the β domain periodicity is 3.39 ± 0.07 nm, which is approximately six times the underlying unreconstructed periodicity. Within all the images the ratio of the α:β periodicity is consistently 2:3. Therefore, the α domain is a (4 × 4) reconstruction and the β domain is a (6 × 6) reconstruction. This is confirmed by the

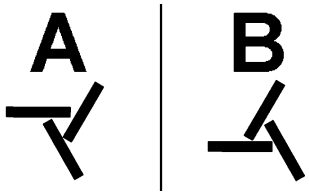

Figure 2. Schematic representation of the features highlighted as A and B in Figure 1b. A and B are non-superimposable mirror images of one another and, thus, result in domains with different chirality.

use of LEED, which shows the distinctive patterns for both reconstructions overlaid. The spots of both patterns tend to be of roughly equal intensity.

The (4 × 4) region in Figure 1b exhibits chirality. Two regions are marked by squares on the (4 × 4) domain. Schematics of these regions (labeled A and B) are shown in Figure 2. These two regions, while being very similar to one another, are not exactly equal. In fact both appear to be "rotating" in opposite directions. They are non-superimposable mirror images of one another and represent two separate chiral domains. One particular chiral domain of the (4 × 4) reconstruction is shown in detail in Figure 1c. Due to the chirality the unit cell does not possess any mirror planes. The reconstruction is also 3-fold rotationally symmetric. The unit cell consists of two distinct halves: one containing the chiral portion; the other a large bright spot. The image shows considerable unit cell detail.

The (6 × 6) reconstruction (β region) in Figure 1b shows an interesting pattern of bright spots. Between consecutively taken images, these sometimes move positions, and sometimes are not present at all. In addition, low bias voltages generally enable the (6 × 6) reconstruction be imaged without these spots. A higher magnification image of the (6 × 6) reconstruction is shown in Figure 1d. On inspection of a unit cell with no bright spots present on it, a mirror plane along the longer diagonal is visible. The unit cell consists of two halves, separated by the shorter diagonal: one containing a darker triangle; one with a triangular arrangement of 6 medium intensity spots. It is this second half where the other bright spots are sometimes observed.

3.2. (5 × 5) Reconstruction. The Ar^+ sputtering time affects the nature of the surface. Ar^+ sputtering for 20 min at 0.5 keV in UHV and then annealing at 1000 °C for 30 min results in STM images like that shown in Figure 3. Figure 3a shows a surface containing only one kind of reconstruction. This reconstruction does not resemble either the (6 × 6) or (4 × 4) reconstruction reported above, and the length of the periodicity is different. Measuring the periodicity reveals it to be 2.70 ± 0.12 nm, which is equivalent to a (5 × 5) reconstruction. This is confirmed using LEED, which gives the characteristic pattern for this reconstruction. The surface consists of large flat continuous terraces with minimal disorder and step heights of 0.224 ± 0.012 nm, which correspond to the d_{111} lattice parameter. The step edges are aligned along the ⟨110⟩ lattice directions. In some images, small regions of the (6 × 6) reconstruction are observed. Figure 3b shows a region of (6 × 6) (indicated by the unit cell in the top left) surrounded by (5 × 5). These (6 × 6) regions have the same periodicity and look the same when imaged at the same bias voltages as the (6 × 6) reported above, reinforcing the view that they are in fact the same (6 × 6) reconstruction. The images in Figure 3, parts b and a, are produced at different bias voltages, and this explains the differences in the appearance of the images. Tip effects can greatly influence the appearance of STM images even when the bias voltage is the same. This effect is shown by the differences between Figure 3, parts a and c. During scanning of an image it is possible for the image to change in appearance from that in Figure 3a to that in Figure 3c, showing that it is due to a change in the nature of the tip. It is likely that one is due to a W atom at the end of the tungsten tip and the other may be caused by an O atom. The (5 × 5) reconstruction has a unit cell with only one mirror plane and 3-fold symmetry.

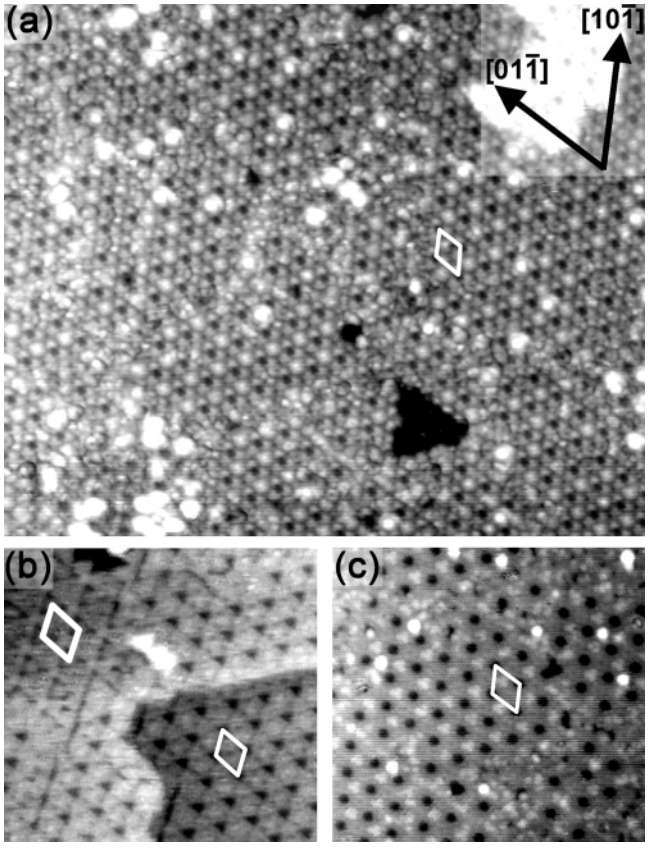

Figure 3. STM images of the (5 × 5) surface showing the effect of different tip and bias conditions. (a) The unit cell is indicated in white. The surface is made up of a number of domains and a small amount of disorder. The majority of the image shows a single terrace (image size 60 × 50 nm^2, sample bias 2.6 V, tunneling current 0.2 nA). (b) Another image of the (5 × 5) reconstruction taken at a bias voltage different from that in (a). The (6 × 6) reconstruction is also imaged and is indicated by the white unit cell with thicker lines in the top left of the image. The (5 × 5) is shown by the slightly smaller white unit cell in the bottom right (image size 25 × 26 nm^2, sample bias 1.0 V, tunneling current 0.1 nA). (c) A further image of the (5 × 5) reconstruction taken under the same conditions as (a). The image shows the effect of a change in the tip. It is assumed that the tip now has a different apical atom. A (5 × 5) unit cell is indicated in white (image size 28 × 30 nm^2, sample bias 2.6 V, tunneling current 0.2 nA).

3.3. (3 × 3) Reconstruction. In order to observe the effect of annealing in different atmospheric conditions, samples are sputtered for 10 min at 500 eV and then annealed for 5 h at 1150 °C in 4.0 × 10^{-4} Pa O_2. Investigation using STM produces the images in Figure 4. Figure 4a shows an STM image showing two large terraces of the (3 × 3) reconstruction. The lattice parameter of the reconstruction in the image is 1.69 ± 0.06 nm which is consistent with a (3 × 3) reconstruction. The reconstruction is also confirmed by LEED. These two terraces are separated by a step of height 0.22 nm, which corresponds to the d_{111} lattice parameter. The step edge is straight and is aligned along the ⟨110⟩ direction, and small kinks can be seen in the step edge when it shifts by a (3 × 3) unit cell width. The (3 × 3) reconstruction can be seen to be a network of bright spots each connected to all adjacent spots by a bright line. The

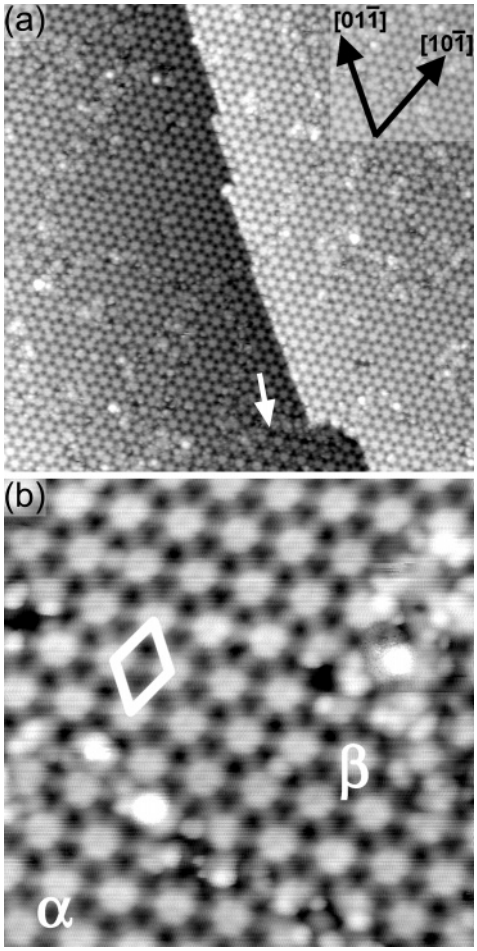

Figure 4. (a) STM image of the (3 × 3) reconstruction. The image shows two terraces with a step edge between them. The step edge follows the ⟨110⟩ direction. The white arrow points to a small region of (4 × 4) reconstruction sitting within the majority (3 × 3) surface (image size 67 × 67 nm^2, sample bias 2.0 V, tunneling current 0.4 nA). (b) High-resolution image of the (3 × 3) reconstruction with the unit cell indicated by a white rhombus. α and *β* indicate two domains shifted by one bulk unit cell relative to one another (image size 14 × 14 nm^2, sample bias 2.0 V, tunneling current 0.4 nA).

(3 × 3) domains tend to be shaped randomly, with each surrounded by a small amount of disorder. The interface between the (3 × 3) domains is caused by the two domains being shifted by a single bulk unit cell relative to one another. Toward the bottom of the image is a small region of (4 × 4) reconstruction, as indicated by the white arrow in the figure. This reconstruction forms under conditions similar to those for the (3 × 3), and it is not unusual to obtain both reconstructions together.

Figure 4b presents a higher magnification image showing the (3 × 3) reconstruction. The unit cell is indicated in the figure by the white rhombus. Here the structure of the reconstructed unit cell can be seen more clearly, along with the disorder present at the domain boundaries. Two domains (α and *β*) are indicated on the image. These are exactly the same except that they are shifted by a single bulk unit cell relative to one another. This causes the disorder which appears between them.

3.4. (9/5 × 9/5) Reconstruction. The effects of annealing samples ex-situ can also be investigated. Samples are first sputtered for 10 min at 0.5 keV in the UHV chamber and then removed and annealed in a mullite furnace tube for 10 h at 1100 °C, with a temperature ramping speed of 500 °C/h for both the increase and decrease of temperature. Pure air (80:20 N_2:O_2 mix) is passed through the tube at atmospheric pressure

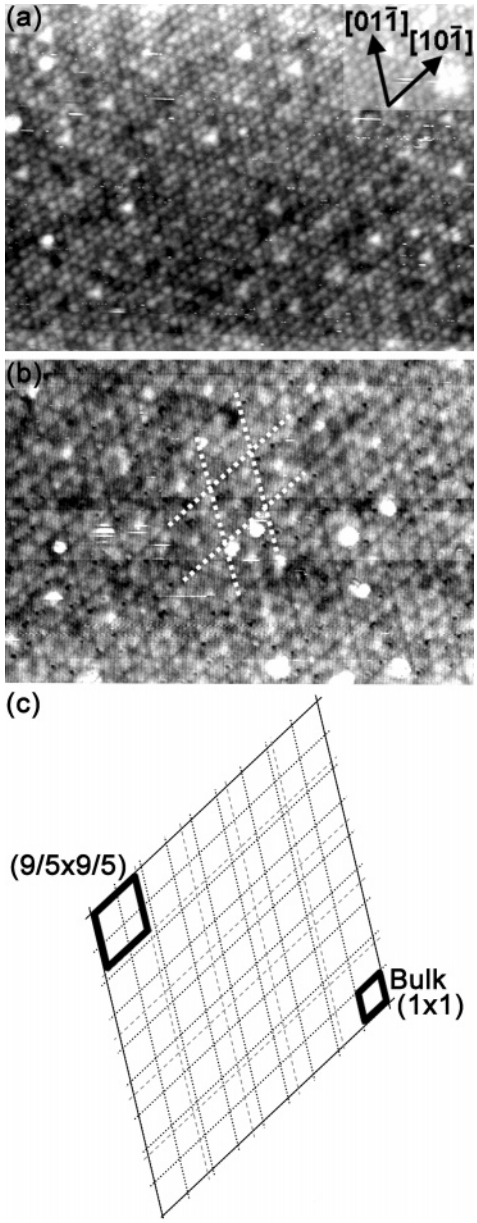

Figure 5. (a) STM image of the (9/5 × 9/5) surface with each unit cell indicated by a single dot (image size 42 × 32 nm^2, sample bias 2.0 V, tunneling current 0.1 nA). (b) Similar image of the (9/5 × 9/5) reconstruction but under different tip conditions (possibly due to a different apical tip atom) leading to the imaging of trenches on the surface. These trenches are indicated by the white dotted lines. The trenches are separated by a distance equivalent to nine bulk terminated unit cells or five reconstructed unit cells (image size 41 × 28 nm^2, sample bias 2.0 V, tunneling current 0.1 nA). (c) Schematic to show the incommensurate nature of the (9/5 × 9/ 5) surface. The schematic is arranged to coincide with the lattice of the images in (a) and (b). The black dotted lines represent the unit cells of the bulk termination (also indicated by the black smaller rhombus), and the gray dashed lines are the (9/5 × 9/5) reconstruction (also indicated by the larger black rhombus). The diagram shows that nine bulk terminated unit cells are equivalent to five (9/5 × 9/5) unit cells. The black unbroken lines show the period over which the two are commensurate (every five (9/5 × 9/5) unit cells or nine bulk unit cells) and represent the points where the trenches occur in (b).

during annealing. On introduction to the STM, the resulting images show a surface which is very rough over a large proportion of its area but with large flat regions of a reconstruction within it. One of these regions is shown in Figure 5. Figure 5a,b shows two images of this surface but with a change in the nature of the tip, resulting in differences in contrast. The

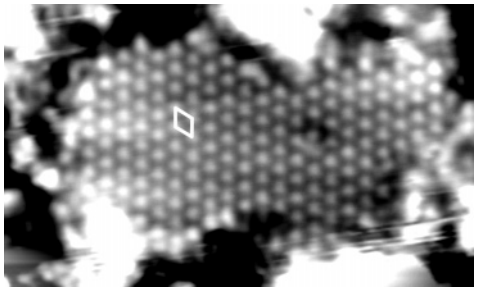

Figure 6. STM image of the TiO nanophase. The white rhombus shows a unit cell represented on the surface. This unit cell has a (2 × 2) periodicity with respect to the TiO(111) bulk terminated periodicity (image size 14 × 8.5 nm^2, sample bias −1.0 V, tunneling current 0.5 nA).

periodicity of the reconstruction is shown in Figure 5a with each dot associated with a unit cell. The periodicity is 0.97 ± 0.04 nm, which is slightly less than two times that of the bulk reconstruction. Figure 5b shows different features of the reconstruction. This image has trenches visible which are separated by a distance five times the periodicity of the reconstructed unit cell. They are also separated by a distance nine times the periodicity of the underlying bulk termination. On investigation of the LEED patterns, it resembles the pattern of a (2 × 2) reconstruction but with the noninteger spots positioned slightly further out (i.e., their reciprocal lattice vector is larger) than they would appear in a (2 × 2) pattern. All these factors indicate that this surface has a (9/5 × 9/5) periodicity.

The (9/5 × 9/5) structure is incommensurate with the underlying periodicity. That is to say the vector for the reconstructed periodicity is not an integer multiple of that of the unreconstructed (1 × 1) periodicity. In Figure 5a the structure of the surface is shown with little effect from the underlying periodicity of the subsurface layers. Each unit cell is indicated by a dot, and all appear to be equivalent. Figure 5b however has more influence from the underlying bulk layers, and the trenches occur when the periodicity of the (9/5 × 9/5) reconstruction and that of the underlying bulk are commensurate. This occurs, as indicated in Figure 5c, at a length of five reconstructed unit cells. This is because five reconstructed unit cells are equivalent in length to nine bulk terminated unit cells, which is an integer multiple of the underlying periodicity.

The surface is mostly formed of large, continuous flat terraces, with very little disorder and large single domains. Step edges were uncommon but were imaged. Step edges are found to have a height of 0.219 ± 0.014 nm, which is equivalent to the d_{111} lattice parameter.

3.5. High-Temperature TiO(111)-(2 × 2) Nanophase. Annealing samples at temperatures above 1400 °C in UHV causes the samples to became very rough. However, small regions are flat and ordered. Figure 6 shows such a region which is produced when samples are annealed in UHV at 1400 °C. The shape of the region is irregular with the edges of the domain following no particular crystallographic directions of the $SrTiO_3$ substrate. The reconstruction can be imaged at biases close to zero and at both negative and positive bias, which indicates a conducting surface. This, and further evidence in the following AES section, suggest that the ordered domains represent a TiO phase. The periodicity of reconstruction is 0.59 nm. However, the (1 × 1) periodicity for a TiO(111) surface is 0.30 nm. This means that the periodicity present, if it is indeed TiO, must be that of a TiO(111)-(2 × 2) reconstruction. This makes sense as it is well-known that the polar (111) surfaces of rock salt type materials can be stabilized by the adoption of an octopolar reconstruction[15] which has a (2 × 2) periodicity. However, without further evidence it is impossible to confirm whether the (2 × 2) reconstruction present on this surface is indeed the octopolar reconstruction or another type of reconstruction with the same overall periodicity.

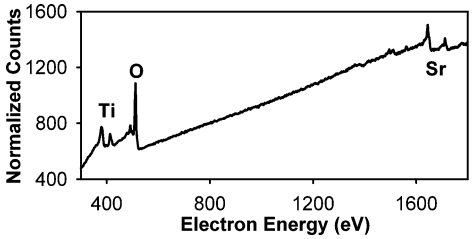

Figure 7. AES spectrum for $SrTiO_3$ formed by cleaving the sample in UHV. This shows the typical features for a $SrTiO_3$ AES spectrum. The O, Ti, and Sr peaks are indicated. The flat region between 600 and 1400 eV is the featureless background which is used for normalization. The AES spectra are normalized to a midpoint on that featureless background of 1000 counts at 1100 eV.

3.6. Auger Electron Spectroscopy (AES). AES spectra were obtained for all the surfaces observed. This was done using an electron beam current of 0.9 μA and an SEM accelerating voltage of 12 kV. Our procedure involves producing an initial rapid low-resolution Auger spectrum (which takes around 10 min), followed by a series of high-resolution scans (taking in total 2−3 h), which are then averaged. Usually the initial scan and the later high-resolution scans match very well in terms of peak heights and energies, and so we can assume that there has been relatively little beam shift or specimen damage.

A typical AES spectrum for $SrTiO_3$ is shown in Figure 7. This spectrum is that for an in-situ cleaved $SrTiO_3$ sample. The peaks at 380 and 413 eV (LMM) are due to the presence of Ti in the surface region. Similarly the peaks at 492 and 511 eV (KLL) are characteristic of O, and Sr is signified by peaks at 1644 and 1711 eV (LMM). The spectrum also contains a featureless background, which has a relatively constant gradient, in the region 600−1400 eV. This is present in all Auger spectra from $SrTiO_3$ surfaces, and though it is a function of the beam current, accelerating voltage, and the geometry of the surface relative to the detector, it is thought to be independent of the nature of the surface. Hence, it is assumed that the featureless background can be taken as a reference. All spectra are scaled so that their featureless backgrounds overlap and are then normalized so that they have an intensity of 1000 counts at 1100 eV (a point in the center of the featureless background). In order for comparisons of chemical composition to be made, it is assumed that UHV cleavage produces a surface which is as close to $SrTiO_3$ stoichiometry as possible.

By comparison of the peak heights of the normalized spectra for the (111) and cleaved surfaces, the concentrations of Sr, Ti, and O were calculated. The normalized spectra for each of the reconstructions compared to that of the cleaved surface are shown in Figure 8. The spectra show that all the (111) surfaces have Ti peaks that are higher than those for the cleaved surface. The TiO (111)-(2 × 2) nanophase has by far the largest Ti peaks and is thus most Ti-enriched, and the (9/5 × 9/5) reconstruction has Ti peaks similar to those for the stoichiometric spectrum and is the least Ti-enriched. In addition, all the surfaces show Sr peaks either similar to, or lower than, those for the stoichiometric spectrum. The (9/5 × 9/5), (3 × 3), and (5 × 5) all have Sr peaks similar to that of the cleaved surface, indicating close to stoichiometric Sr concentration, whereas that for the (4 × 4)/(6 × 6) reconstruction is slightly smaller, and the TiO (111)-(2 × 2) nanophase spectrum has almost no Sr peak at all.

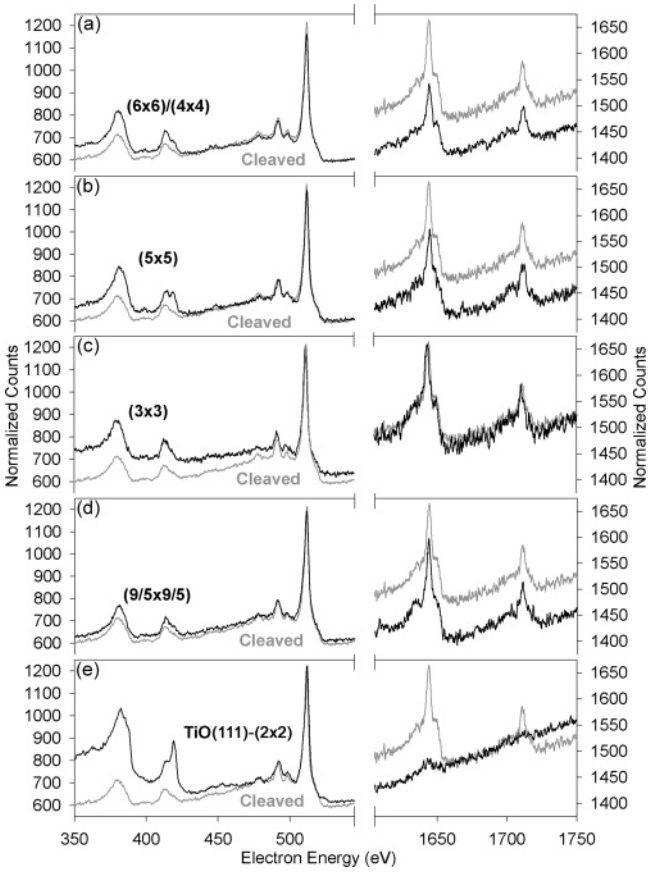

Figure 8. AES spectra for the $SrTiO_3(111)$ reconstructions compared to that of the cleaved surface. (a) Spectra are shown of the (4 × 4)/(6 × 6) and cleaved surfaces. This shows an enrichment of Ti and deficiency in both Sr and O. (b) Spectra are shown of the (5 × 5) and cleaved surfaces. The Ti peaks for (5 × 5) are greater than those for the cleaved surface, and so (5 × 5) is Ti enriched. O and Sr are close to stoichiometry. (c) Spectra are shown of the (3 × 3) and cleaved surfaces. The Ti peaks are larger for the (3 × 3) spectrum than for the stoichiometric spectrum. The O and Sr peaks for both are similar. (d) Spectra are shown of the (9/5 × 9/5) and cleaved surfaces. All the peaks of the (9/5 × 9/5) spectrum are similar to those for the stoichiometric surface. Ti is, however, slightly enriched in the (9/5 × 9/5) surface. (e) Spectra are shown of the TiO (111)-(2 × 2) nanophase and cleaved surfaces. The Ti peaks for the TiO (111)-(2 × 2) nanophase are much greater than those for the stoichiometric surface. In addition the position of the peak at 413 eV in the stoichiometric spectrum has shifted to higher energy in the TiO(111)-(2 × 2) spectrum. The Sr peaks in the TiO(111)-(2 × 2) spectrum are almost completely absent.

The normalized peak heights for the cleaved spectrum are taken to indicate a stoichiometric surface, and so the relative Sr, Ti, and O concentrations are assumed to be 1, 1, and 3, respectively. The peak heights for the other surfaces are then obtained and their values compared to those of the cleaved surface to give absolute concentrations of each species. This gives the results in Table 1. The Auger peak energies used to determine the relative fractions of Sr, Ti, and O are at 1644, 380, and 511 eV, respectively. These energies correspond to inelastic mean free paths of around 2.0, 1.0, and 1.1 nm, respectively. This indicates a depth probed down to ~3 unit cells for Ti and O and around 5 unit cells for Sr. The depth of the reconstruction where there is a significant amount of nonstoichiometry is unlikely to be greater than 1 unit cell. We can therefore state that certainly less than half of the Auger spectrum actually reflects the composition of the reconstruction. Here we will not attempt to determine the stoichiometries of the reconstructions but rather use the AES data to determine which surfaces are relatively rich or poor in Ti, O, and Sr.

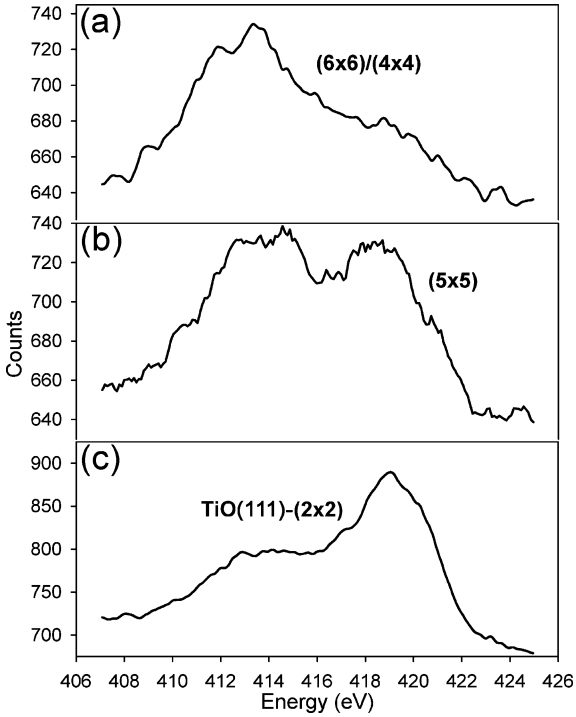

Figure 9. Ti (LLM) Auger spectra between 406 and 426 eV. (a) The spectrum of the (6 × 6)/(4 × 4) reconstruction is presented. This shows a peak on the left-hand side at lower energy (413 eV), with a shoulder on the right-hand side at higher energy (419 eV). This is the characteristic peak shape for Ti^{4+} being present within the surface region. (b) A spectrum of the (5 × 5) reconstruction is presented. This shows two distinct peaks at 413 and 419 eV. (c) The spectrum of the TiO(111)-(2 × 2) nanophase is presented. The peak is on the right-hand side at higher energy (419 eV), with a shoulder at lower energy (413 eV). This is the characteristic fingerprint of Ti^{2+} being present in the surface region.

TABLE 1: Concentrations of Each Species in the $SrTiO_3(111)$ Reconstructions[a]

reconstruction	Ti	O	Sr	O/Ti	Ti/Sr
TiO(111)-(2 × 2)	3.23	2.91	0.15	0.90	N/A
(5 × 5)	1.98	2.78	0.88	1.40	2.26
(6 × 6)/(4 × 4)	1.74	2.73	0.72	1.56	2.43
(3 × 3)	1.63	2.74	1.05	1.68	1.56
(9/5 × 9/5)	1.26	2.74	1.02	2.18	1.24
cleaved	1.00	3.00	1.00	3.00	1.00

[a] They are calculated by comparing the peak heights from the normalized AES spectra of the reconstructed samples to that of the cleaved stoichiometric sample. The TiO (111)-(2 × 2) nanophase represents the most Ti-enriched phase. It has negligible Sr, and the O and Ti concentrations are approximately equal, confirming TiO stoichiometry. Of the ($n \times n$) family of reconstructions, the (5 × 5) is the most Ti enriched, followed by (6 × 6)/(4 × 4) and (3 × 3). All have Sr either somewhat depleted or stoichiometric. The O/Ti ratio for the ($n \times n$) family shows the highest value for (3 × 3), indicating it is the most O enriched, and the lowest for (5 × 5), showing it to be the most O depleted. The (9/5 × 9/5) reconstruction has the lowest Ti enrichment of all the reconstructions and is also the most O enriched as it has the highest O/Ti ratio.

Table 1 shows that the most Ti-enriched surface is the TiO-(111)-(2 × 2) nanophase, followed by the (5 × 5), (6 × 6)/(4 × 4), and (3 × 3) reconstructions. The (9/5 × 9/5) reconstruction is the least Ti-enriched. All the reconstructions are close to stoichiometry for Sr except the (6 × 6)/(4 × 4) reconstruction, which is slightly deficient, and the TiO(111)-(2 × 2) nanophase, which contains very little Sr. The oxygen concentration is best

considered by looking at the O/Ti ratio, as Ti is the dominant surface species, and this ratio gives an indication of how oxygen deficient or enriched the surfaces are. These suggest sensibly that the (9/5 × 9/5) surface is the most oxygen-enriched and that the TiO(111)-(2 × 2) nanophase is highly reduced.

A further interesting feature is seen on the TiO(111)-(2 × 2) Auger spectrum. Figure 9 shows the Ti peak at 413 eV for the (6 × 6)/(4 × 4) reconstructions (Figure 9a), the (5 × 5) reconstruction (Figure 9b), and the TiO(111)-(2 × 2) nanophase (Figure 9c). Both the TiO (111)-(2 × 2) and (6 × 6)/(4 × 4) spectra show a main peak with a shoulder. However, the (6 × 6) peak has the shoulder on the right-hand side at higher energy, whereas the TiO(111)-(2 × 2) surface has the shoulder on the left-hand side at an energy lower than that of the main peak. The (5 × 5) spectra contains two closely positioned peaks both positioned at the same energy as the main peaks in the TiO-(111)-(2 × 2) and (6 × 6)/(4 × 4) spectra. This change in shape of the spectrum between 406 and 426 eV is due to varying oxidation states of the Ti. It has previously been shown that the characteristic peak shape of a Ti^{4+} Auger peak has a main peak at 413 eV and a shoulder at 419 eV,[7,16] whereas the signature of a Ti^{2+} species is an Auger spectrum with a main peak at 419 eV and a shoulder at 413 eV. Hence, the (6 × 6) surface contains Ti^{4+} as its dominant species, and the TiO (111)-(2 × 2) nanophase contains Ti^{2+} in greatest concentration. The (5 × 5) spectrum has equally sized peaks at 413 and 419 eV. It is possible that this is due to both Ti^{2+} and Ti^{4+} being present and that the characteristic Auger peaks for both species overlap producing the double peak observed. Also, it may be due to that being the characteristic Auger peak shape for Ti^{3+} ions. Either way, it shows that the (5 × 5) surface represents a more reduced phase, as it contains Ti in oxidation states other than the Ti^{4+} state characteristic for $SrTiO_3$.

None of the Auger spectra showed any peaks due to Nb. The concentration of Nb was thus too low to be detected. The possibility of significant Nb segregation to the surface can thus be discounted, and it is unlikely that Nb is responsible for the stabilization of the surface reconstructions.

4. Discussion

The majority of reconstructions observed in this paper represent a family of ($n \times n$) type surfaces. The (3 × 3), (4 × 4), (5 × 5), and (6 × 6) reconstructions are all observed to coexist with other members of the family, suggesting they are all of similar composition and surface energies. They are all formed from a similar starting point: a surface that has been heavily disordered by sputtering (although the surface which produces the (5 × 5) reconstruction is sputtered for longer). On annealing of these sputtered surfaces, the disordered top layer recrystallizes forming the reconstruction in the uppermost layers. The more a surface is sputtered, the more oxygen deficient it is likely to become, as sputtering with Ar ions can easily remove O from the $SrTiO_3$ lattice in the surface layers. This suggests that the (5 × 5) surface will represent the most oxygen depleted surface of the family of ($n \times n$) reconstructions as it forms when the surface is subjected to the greatest sputtering time. The (6 × 6) reconstruction is sometimes seen to coexist with the (5 × 5) surface, and so it is likely that these two reconstructions represent a similar level of surface oxygen depletion and composition. No other reconstruction is found to coexist with the (5 × 5), but the (4 × 4) and (6 × 6) reconstructions are almost always found to exist together, again suggesting that they have similar levels oxygen deficiency, composition, and energy. The (3 × 3) reconstruction is clearly the least oxygen-depleted surface of the ($n \times n$) family of reconstructions, as it forms in the most oxygen-rich conditions (a low pressure of oxygen rather than UHV). Again, the (3 × 3) reconstruction only coexists with the (4 × 4) reconstruction, suggesting that the (4 × 4) surface must be a relatively less oxygen depleted state than the (6 × 6) surface as this cannot form alongside the (3 × 3) reconstruction. These results allow us to order the relative oxygen concentration levels of all the ($n \times n$) family of reconstructions: most oxygen depleted, (5 × 5) < (6 × 6) < (4 × 4) < (3 × 3), most oxygen enriched.

AES analysis also confirms the relative oxygen depletion levels. By considering the O/Ti ratio, one can determine the oxygen concentration of the surface. The Sr level is not as variable as that of Ti, and thus, it can be ignored for this comparison. The (3 × 3) surface has the highest O/Ti ratio (1.68) of the ($n \times n$) family indicating that it is the most oxygen enriched. Similarly the (6 × 6)/(4 × 4) O/Ti ratio is a little lower at 1.56 and the ratio for the (5 × 5) is the lowest at 1.40, indicating it is the most oxygen depleted. This confirms the order of oxygen depletion and enrichment stated above.

The (9/5 × 9/5) surface most likely represents the most oxygen-enriched phase on the $SrTiO_3$(111) surface because it forms under atmospheric pressures of air and is never observed to form in the chamber by annealing either in UHV or in low oxygen pressures. This is confirmed by the O/Ti ratio, which at 2.18 is the highest for all the surfaces covered in this paper. The noncommensurate nature of this surface is unusual. It suggests that the surface structure is relatively independent of the underlying periodicity of the bulk, as it seems to maintain the same arrangement in every unit cell, despite the fact that the structure of the bulk beneath each individual unit cell will differ. Step edges are not common on the (9/5 × 9/5) surface, but when they are observed, they followed the ⟨110⟩ directions. This may be due to the fact that step edges are only energetically favorable when both the overlying reconstruction and underlying bulk periodicities coincide.

Conversely the TiO (111)-(2 × 2) structure is highly reduced. This is shown by the AES spectrum which indicates a very low O/Ti ratio, with roughly equal amounts of Ti and O being present. This is consistent with the surface being TiO enriched. The shape of the AES spectrum between 406 and 426 eV also shows that Ti^{2+} is the dominant Ti species. The small Sr peaks in the spectrum is further evidence that the surface is highly TiO enriched. None of the reconstructions mentioned in this paper, except that of the TiO(111)-(2 × 2) overlayer, can be imaged at biases close to zero. The (3 × 3) and (4 × 4) reconstructions cannot be imaged at biases of less than +1.0 V, whereas the (6 × 6) and (5 × 5) surfaces can be imaged at lower biases but not at less than +0.8 V. None can be imaged at negative bias except the TiO(111)-(2 × 2) nanophase. As the TiO(111)-(2 × 2) surface can be imaged at all biases, this confirms that the TiO surface layers are metallic; i.e., they have no gap at the Fermi level. At positive bias, images are produced via electrons tunneling from the tip to a particular state, in the sample, above the Fermi level. The closer the bias is to zero, the closer the state tunneled into is to the Fermi level, and so if no states exist close to the Fermi level, imaging cannot occur at biases close to zero. TiO is known to be an electrical conductor, and so this property provides additional proof of the presence of Ti^{2+}. This, the lattice parameter, the presence of a Ti^{2+} peak in the AES spectrum, and the relative O and Ti concentrations all indicate that there is a TiO(111)-(2 × 2) nanophase present on the surface. This is unsurprising since the surface has been annealed at very high temperatures in UHV.

Such an environment is very reducing. It is likely that O is lost from the surface during the annealing process to such an extent that phase separation occurs. The phases left in this reduced structure may be Sr and TiO. The Sr could then be lost via sublimation as Sr has a low boiling point in UHV. This would result in TiO remaining on the surface. The production of a metallic surface phase will also allow the cancellation of polarity, as electrons in the surface will be free to redistribute themselves in response to the polar electric field, quenching it.

We believe from work on the $SrTiO_3$(001) surface, that Ar^+ sputtering increases the mobility of the Ti within the surface region and that annealing in conjunction with that increased mobility allows the Ti to move to the surface. O ions are known to be very mobile within $SrTiO_3$, as annealing causes the production of O vacancies in the bulk. In extreme cases, O may sublime into the vacuum, reducing the sample. Likewise it is also possible that O could be incorporated into the structure from the atmosphere when annealed under oxygen-rich conditions. All the reconstructions are Ti enriched in comparison to that of a cleaved stoichiometric surface. All are also either Sr deficient or have Sr concentrations similar to stoichiometry. This suggests that in all cases a TiO_x phase has formed on the uppermost surface layers, and it is that which is responsible for the reconstruction. To do this, Ti will diffuse from the bulk. The type of TiO_x reconstruction adopted is then dependent upon the nature of the initial sputtered surface (i.e., how aggressively it has been bombarded), the oxidizing conditions it is annealed in, and the anneal time and temperature.

The AES data show that the more oxygen-depleted surfaces have a higher concentration of Ti than the more oxygen-enriched surfaces. The (9/5 × 9/5) reconstruction has the lowest Ti concentration at 1.26. Correspondingly, (3 × 3), (6 × 6)/(4 × 4), (5 × 5), and TiO(111)-(2 × 2) have Ti concentrations of 1.68, 1.74, 1.98, and 3.23, respectively, showing the increase in Ti with oxygen depletion. This suggests also that greater sputtering, higher temperatures, and annealing in lower pressure of O_2 are all factors which increase the tendency of TiO_x to form at the surface.

No Nb Auger peaks were observed in any of the AES spectra. It is therefore unlikely that any of the surfaces represent any sort of Nb enrichment or surface phase, or that the Nb doping plays any role in stabilizing a surface structure which would otherwise be unfavorable. However, one way in which the surface may be affected by Nb is by increasing the electrical conductivity of the sample. The distribution of conduction electrons can be used as a mechanism to help neutralize the surface dipole, hence leading to the possibility of surface structures that would not be stable in an insulating sample. However, annealing $SrTiO_3$ in reducing conditions produces O vacancies which also dope n-type and would produce an effect similar to Nb doping. Therefore, it is likely that Nb doping does nothing more than simulating a heavily reduced crystal.

5. Conclusions

A family of ($n \times n$) reconstructions can be produced by Ar^+ sputtering and then annealing the $SrTiO_3$(111) surface. The (3 × 3) reconstruction represents the most oxygen-enriched surface, followed by (4 × 4) and (6 × 6), with (5 × 5) the most oxygen-depleted ($n \times n$) reconstruction. Annealing in atmospheric air produces a highly oxygen enriched (9/5 × 9/5) reconstruction, and annealing at high temperatures in vacuum forms a very reduced TiO(111)-(2 × 2) nanophase on the surface. None of these surfaces are electrically conducting apart from the TiO-(111)-(2 × 2) nanophase which contains Ti^{2+} ions. Annealing in lower pressures of O_2, longer Ar^+ sputtering, and higher temperatures all contribute to greater oxygen depletion of the (111) surface. The more oxygen depleted the surface, the higher the concentration of Ti at the surface. $SrTiO_3$(111) represents a paradox in the field of polar surfaces. Far from being impossible as some theories would predict, it actually forms a large variety of different stable terminations.

Acknowledgment. We thank D. T. Newell for allowing the reproduction of his UHV cleaved Auger data and Chris Spencer (JEOL U.K.) for his technical support. We are also grateful to L. D. Marks and A. N. Chiaramonti for their valuable guidance in the preparation of some of the reconstructions shown here. The Ph.D. thesis of A. N. Chiaramonti also covers some of the observations described in this paper.[17] We thank the EPSRC for funding.

References and Notes

(1) Tasker, P. W. *J. Phys. C* **1979**, *12*, 4977.

(2) Noguera, C. *J. Phys.: Condens. Matter* **2000**, *12*, R367.

(3) Russell, B. C.; Castell, M. R. *Phys. Rev. B* **2007**, *75*, 155433.

(4) Haruyama, Y.; Aiura, Y.; Bando, H.; Nishihara, Y.; Kato, H. *J. Electron Spectrosc. Relat. Phenom.* **1998**, *88*−*91*, 695.

(5) Sekiguchi, S.; Fujimoto, M.; Kang, M. G.; Koizumi, S.; Cho, S. B.; Tanaka, J. *Jpn. J. Appl. Phys.* **1998**, *37*, 4140.

(6) Sekiguchi, S.; Fujimoto, M.; Nomura, M.; Cho, S. B.; Tanaka, J.; Nishihara, T.; Kang, M. G.; Park, H. H. *Solid State Ionics* **1998**, *108*, 73.

(7) Lo, W. J.; Somorjai, G. A. *Phys. Rev. B* **1978**, *17*, 4943.

(8) Marsh, H. L.; Deak, D. S.; Silly, F.; Kirkland, A. I.; Castell, M. R. *Nanotechnology* **2006**, *17*, 3543.

(9) Deak, D. S.; Silly, F.; Newell, D. T.; Castell, M. R. *J. Phys. Chem. B* **2006**, *110*, 9246.

(10) Castell, M. R. *Surf. Sci.* **2002**, *516*, 33.

(11) Erdman, N.; Marks, L. D.; Poeppelmeier, K. R.; Asta, M.; Warschkow, O.; Ellis, D. E. *J. Am. Chem. Soc.* **2003**, *125*, 10050.

(12) Castell, M. R. *Surf. Sci.* **2002**, *505*, 1.

(13) Silly, F.; Castell, M. R. *Appl. Phys. Lett.* **2004**, *85*, 3223.

(14) Noland, J. A. *Phys. Rev.* **1954**, *94*, 724.

(15) Wolf, D. *Phys. Rev. Lett.* **1992**, *68*, 3315.

(16) Newell, D. T.; Harrison, A.; Silly, F.; Castell, M. R. *Phys. Rev. B* **2007**, *75*, 205429.

(17) Chiaramonti, A. N. Ph.D. Thesis, Northwestern University, Evanston, IL 60208, 2005.